Ocean Boundary Mixing during Ekman Layer Arrest

Scott A. Condie

CSIRO Marine Research, Hobart, Tasmania, Australia

ABSTRACT

As a water parcel comes into contact with an ocean boundary, energy is dissipated within the boundary layer with some fraction directed into vertical mixing. In a stratified flow this increases the potential energy associated with the density field. It has previously been assumed that mixing efficiencies (ratio of potential energy increase to total energy dissipation) are likely to be small (<10%), which would also imply that boundary mixing is a minor contributor to total ocean mixing. While this is probably true for mixing driven purely by shear driven instability of the boundary layer, the analysis presented here suggests that flows with downslope Ekman transport can generate much larger mixing efficiencies. This is supported by laboratory experiments, which yield mixing efficiencies of 30% (independent of flow parameters), compared to around 3% for flows in the same system with upslope Ekman transport. Simple basinwide estimates suggest that this mechanism can potentially account for a significant fraction of the vertical mixing in the ocean.

1. Introduction

Identifying the major sources of ocean mixing has been a central issue since Munk (1966) suggested that an average vertical eddy diffusivity of order 10^{-4} m^2 s^{-1} is required to balance the vertical ocean heat flux. In more recent times it has been recognized that much of the ocean is directly ventilated to the atmosphere, so the thermocline structure can be explained in terms of isopycnal advection and the lower levels of diffusion (10^{-5} m^2 s^{-1}) obtained from direct measurements of microstructure (Gregg 1987, 1989) and diffusion of passive tracers (Ledwell et al. 1993; Matear and Wong 1997). However, enhanced diffusivities still appear to be an essential component of the deep ocean balance, particularly for conversion of bottom water into deep water. Strong interior mixing ($>10^{-4}$ m^2 s^{-1}) has recently been inferred from microstructure measurements over rough topography in the deep Brazil Basin and attributed to internal wave breaking (Polzin et al. 1997). However, the same measurements over the abyssal plain yield diffusivities of order 10^{-5} m^2 s^{-1}, and the basinwide contribution of internal wave breaking is still difficult to quantify.

Munk first suggested that mixing may be concentrated around ocean boundaries and this has been investigated in more detail by Armi (1978, 1979) and Ivey (1987). A first estimate of the potential contribution of boundary

Corresponding author address: Dr. Scott A. Condie, CSIRO Marine Research, GPO Box 1538, Hobart, Tasmania 7001, Australia.
E-mail: scott.condie@marine.csiro.au

mixing can be obtained by following the arguments presented by Garrett and Gilbert (1988) and Garrett (1990). The rate of energy dissipation per unit area of seafloor is usually parameterized as $\rho C_D u^3$, where ρ is the water density, $C_D = 2.5 \times 10^{-3}$ is the drag coefficient, and u is the bottom velocity. The rate of potential energy increase per unit area due to boundary mixing is then given by $\Gamma \rho C_D u^3$, where the mixing efficiency Γ is defined as the fraction of energy dissipation, which appears as increased potential energy of the density field. The second quantity required is the rate of potential energy increase per unit volume of ocean interior. This can be represented by $\rho \kappa_v N^2$, where κ_v is the average vertical diffusivity which incorporates nonlocal processes such as boundary mixing, and $N^2 = -g(\partial \rho / \partial z)/\rho$ is the buoyancy frequency where g is the gravitational acceleration (Garrett and Gilbert 1988). For any interior density layer we can now integrate the boundary mixing term over the area in contact with the boundary, and the interior mixing term over the entire volume of the layer. Equating these terms then gives

$$\kappa_v = \frac{\Gamma C_D u^3}{N^2} \frac{A_{\text{bdy}}}{A_{\text{tot}} h}, \tag{1}$$

where $A_{\text{bdy}}(z, h)$ is the boundary area in contact with the layer, $A_{\text{tot}}(z)$ is the total area of the layer, and h is the boundary layer depth (Garrett and Gilbert 1988; Garrett 1990).

Equation (1) can be used to estimate the boundary mixing efficiency required to account for an average diffusivity of say $\kappa_v \approx 10^{-4}$ m^2 s^{-1}. Appropriate parameters for the deep ocean are $N \approx 10^{-3}$ s^{-1} and $A_{\text{bdy}}/$

$A_{\text{tot}}h \approx 3 \times 10^{-4}$ m^{-1} (Armi 1979) so that a bottom velocity of $u \approx 0.05$ m s^{-1} implies $\Gamma \approx 1$, while $u \approx 0.1$ m s^{-1} implies $\Gamma \approx 0.1$. While these calculations are necessarily very approximate, they do suggest that relatively large mixing efficiencies ($\Gamma > 0.1$) would be required to explain a significant fraction of ocean mixing in terms of boundary mixing.

One of the major factors thought to limit mixing efficiencies is the exchange of mixed water between the boundary layer and ocean interior (Garrett 1979, 1990). If this occurs more slowly than the mixing process itself, then most of the energy will be directed into mixing an already homogenous boundary layer. It was on this basis that Garrett (1979) argued that boundary mixing was likely to be a minor contributor to κ_v, sighting the Kato and Phillips (1969) laboratory efficiencies of $\Gamma \approx 0.07$ and assuming a value of $\Gamma \approx 0.01$ for well-developed boundary layers.

A number of exchange mechanisms have been proposed, including along-isopycnal transport of boundary mixed water (Munk 1966), separation of the boundary layer controlled by the interior flow (Armi 1978), and shear dispersion along the slope (Phillips et al. 1986). However, the relative contribution of these processes within unsteady oceanic flows is still an open question (see review by Garrett et al. 1993).

The efficiency arguments presented above relate to mixing generated by shear instability within the bottom boundary layer. However, there is a second boundary mixing mechanism associated with the shutdown or arrest of the Ekman layer, which relies on hydrostatic instability to generate mixing. This paper seeks to demonstrate that the latter has far more potential to explain a significant fraction of total ocean mixing.

2. Boundary layer dynamics

When a stratified current moves over a sloping bottom, Ekman pumping tends to be opposed by buoyancy forces, leading to the arrest or shutdown of the Ekman flux. This adjusts the density field toward a state in which the geostrophic alongslope velocity approaches zero near the boundary purely through the thermal wind balance. If the flow direction generates Ekman pumping up the slope, then the process remains statically stable and mixing can only be generated through shear instability. However, downslope pumping leads to static instability, which suggests enhanced mixing. While these boundary layer processes have been studied in some detail (Thorpe 1987; Lentz and Trowbridge 1991; Trowbridge and Lentz 1991; MacCready and Rhines 1991, 1993; Ramsden 1995; Middleton and Ramsden 1996), the implications for ocean mixing have been unclear (Garrett et al. 1993).

Before considering more general ocean mixing questions, it is necessary to first review some recent results on the boundary layer dynamics. Consider a rotating stratified flow of buoyancy frequency N and alongslope
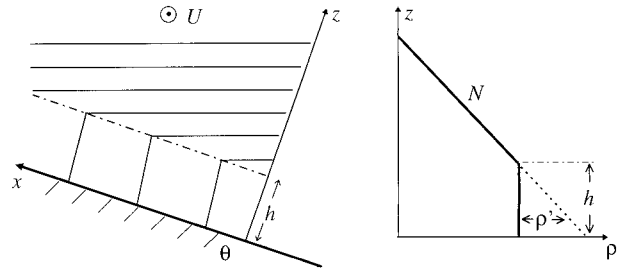

FIG. 1. (a) Schematic side view of the isotherm pattern above the sloping bottom for a downwelling flow with interior alongslope velocity U. (b) The corresponding density profile along the z coordinate, perpendicular to the sloping bottom.

geostrophic velocity $U(z, t)$, moving over a bottom slope of inclination θ. Here t is time and z is the perpendicular distance from the sloping bottom as shown in Fig. 1. As Ekman pumping is shut down by the opposing buoyancy forces, the density field adjusts toward a thermal wind balance with its level of no motion at the boundary (MacCready and Rhines 1991; Trowbridge and Lentz 1991). It is this time-dependent adjustment of downwelling Ekman layers that is most significant for mixing.

Ramsden (1995) and Middleton and Ramsden (1996) considered the time-dependent development of the boundary layer in some detail using both theoretical analysis and numerical solutions. These studies showed that the alongslope near-bottom velocity within a downwelling Ekman layer can be expressed as a function of the growing boundary layer height $h(t)$ in the form

$$u = U\left(1 - \frac{h}{h_d}\right), \qquad (2)$$

where

$$h_d = \frac{fU}{N^2 \sin\theta} \qquad (3)$$

is the asymptotic boundary layer depth corresponding to thermal wind with zero flow at the boundary (Trowbridge and Lentz 1991). Ramsden (1995) also derived a differential equation for the development of the mixed layer height,

$$\frac{dt}{t_d} = \frac{hdh}{(h_d - h)^2}, \qquad (4)$$

where

$$t_d = \frac{f^3}{C_D N^4 \sin^3\theta} \qquad (5)$$

is the shutdown timescale for downwelling Ekman layers. The solution to (4) can be written explicitly for t:

$$\frac{t}{t_d} = \frac{h}{h_d - h} - \ln\left(1 - \frac{h}{h_d}\right). \qquad (6)$$

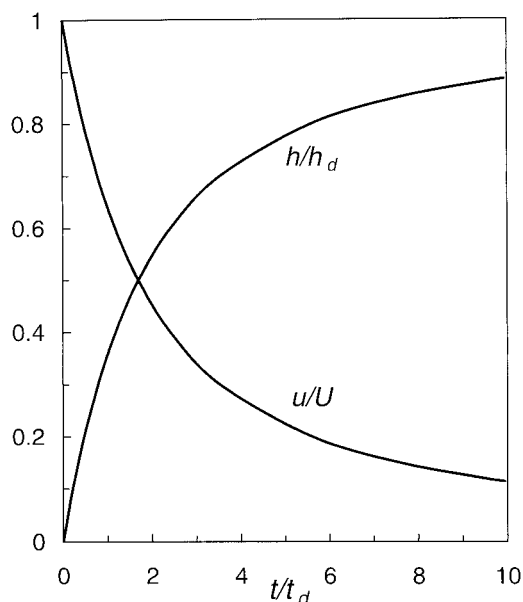The development of the boundary layer height and ve-

FIG. 2. Theoretical estimates for the development of the boundary layer height and velocity for downwelling favorable flows based on the results of Ramsden (1995).

locity are plotted in Fig. 2 for a flow which initially had a uniform alongslope velocity U.

It has already been noted that for any boundary layer mixing mechanism to be effective, exchange with the ocean interior must occur on timescales comparable to the mixing timescale (Garrett 1979, 1990). Figure 2 suggests that most of the mixing associated with downwelling Ekman layers occurs within a few shutdown times ($t < 3t_d$) of the stratified water parcel making contact with the slope. Within the thermocline, t_d is typically of order 10 days, so mixing would be most effective for contact times up to the order of a month. Boundary currents with realistic levels of variability should almost invariably fall within this range, even if we rely only on advective processes such as separation (Armi 1978). In the deeper ocean, t_d is of order 100 days or more so that contact times of a year or more might still be expected to produce effective mixing. The large-scale advective circulation alone would normally satisfy this criteria without even considering eddies and other sources of shorter term variability. It therefore appears that exchange with the ocean interior is not a serious inhibitor to mixing by downwelling Ekman layers.

3. Basinwide energy balance

The boundary layer formulation can now be used to investigate the energetics of mixing by downwelling Ekman layers. A basin-scale balance, similar to that presented above from Garrett (1990), will provide an

estimate of mixing that can be compared to other mixing processes.

Assuming that the density gradient is initially linear, the density anomaly within the boundary layer is given by $\rho' = (h - z)\rho N^2/g$, the factor $\rho N^2/g$ being the size of the density gradient. The corresponding increase in potential energy per unit area is in accordance with Gill (1979, p. 140):

$$\int_0^{h(t)} \frac{1}{2} \frac{g^2 \rho'^2}{\rho N^2} \, dz = \frac{1}{6} \rho N^2 h^3. \qquad (7)$$

The rate of increase of potential energy over the entire density layer can now be estimated by integrating the time derivative of (7) over the boundary contact area of the layer. The equivalent quantity associated with a hypothetical interior diffusivity κ_v is the integral of $\rho \kappa_v N^2$ over the layer volume. Equating these two quantities gives

$$\frac{\partial}{\partial t} \int_{\text{bdy}} \frac{1}{6} \rho N^2 h^3 \, dA = \int_0^h \int_{\text{tot}} \rho \kappa_v N^2 \, dA \, dz, \qquad (8)$$

where dA refers to integration over either the entire density surface (tot) or that part of it in contact with the boundary (bdy). Neglecting along-isopycnal gradients in N, the integrals in (8) can be easily evaluated and combined with (4) to yield an effective diffusivity of

$$\kappa_v = \frac{1}{2} \frac{(h_d - h)^2}{t_d} \frac{\gamma A_{\text{bdy}}}{A_{\text{tot}}}, \qquad (9)$$

where γ is the fraction of the boundary area with downwelling favorable flow (i.e., boundary to the right in the Northern Hemisphere as shown in Fig. 1). It should be emphasized that κ_v is a hypothetical diffusivity that, if applied uniformly throughout the layer, would generate the equivalent amount of mixing to the Ekman shutdown process. It is not related to the local diffusivity within the boundary layer itself.

The effective diffusivity given by (9) is a function of the time that the water parcel is in contact with the boundary through the dependence on $h(t)$. This dependence can be more clearly seen by rewriting (9) in the form

$$\kappa_v' = \frac{1}{2} \left(1 - \frac{h}{h_d} \right)^2, \qquad (10)$$

where for convenience a nondimensional effective diffusivity has been defined as

$$\kappa_v' = \frac{\kappa_v}{C_D U^2 \sin\theta (\gamma A_{\text{bdy}}/A_{\text{tot}})/f}. \qquad (11)$$

This quantity has been calculated from the right-hand side of (10) and plotted as a function of nondimensional time in Fig. 3, along with its cumulative average (i.e., average of κ_v over the time that the fluid parcel has been in contact with the boundary). From this we can estimate the timescales over which water parcels would need to
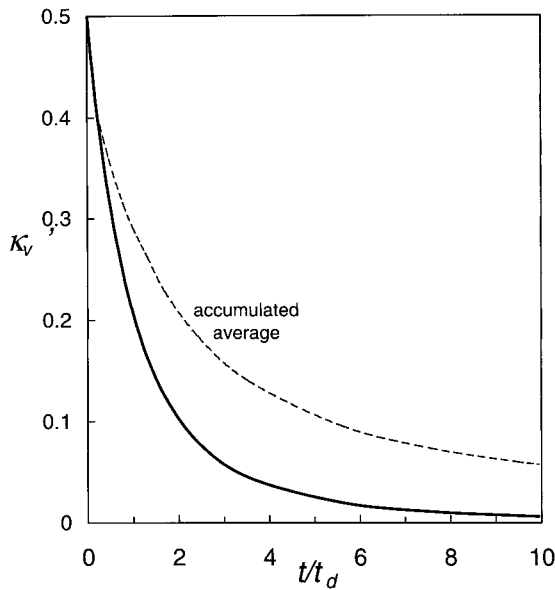
FIG. 3. Development of the nondimensional effective diffusivity associated with boundary mixing in downwelling favorable flows. The cumulative average is the average of κ_v over the time that the fluid parcel has been in contact with the boundary.

TABLE 1. Representative values $A_{\mathrm{bdy}}/A_{\mathrm{tot}}$ for the world's oceans (Armi 1979) for a range of depth intervals. The third column lists the corresponding nondimensional diffusivities based on parameter values of $f = 10^{-4}$ s^{-1}, $\sin\theta = 10^{-2}$, $\gamma = 0.5$, $C_D = 2.5 \times 10^{-3}$, and $U^2/\kappa_v = 10^2$ s^{-1} (the last of which might correspond to $U = 0.1$ m s^{-1} and $\kappa_v = 10^{-4}$ m^2 s^{-1} or $U = 0.03$ m s^{-1} and $\kappa_v = 10^{-5}$ m^2 s^{-1}).

Depth interval (m)	$A_{\mathrm{bdy}}/A_{\mathrm{tot}}$	κ_v'
200–1000	0.03	2.7
1000–2000	0.04	2.0
2000–3000	0.1	0.8
3000–4000	0.3	0.3
4000–5000	0.6	0.1

be in contact with the boundary to contribute significantly to ocean mixing.

To calculate κ_v, the downwelling favorable fraction γ must first be estimated. A value of $\gamma \approx 0.5$ is probably conservative since most of the deep circulation, including deep western boundary currents, tends to be cyclonic and therefore downwelling favorable. Using other representative parameter values, Table 1 illustrates how κ_v' varies with depth based on values of $A_{\mathrm{bdy}}/A_{\mathrm{tot}}(z)$ provided by Armi (1979). These values can be compared with the cumulative average diffusivities in Fig. 3 in order to estimate the potential contribution of downwelling Ekman layers.

As a first example, consider thermocline waters (200–2000 m) where $\kappa_v' \approx 2$ (Table 1). Provided the contact times for fluid parcels are typically not more than few t_d (typically a month for the thermocline), Fig. 3 suggests that downwelling Ekman layers might contribute up to around 15% of κ_v'. Longer contact times would tend to reduce this percentage, while higher values of U^2/κ_v would increase it. For instance, it has been noted previously that the ocean heat balance requires effective diffusivities in the thermocline of around $\kappa_v = 10^{-5}$ m^2 s^{-1}. For downwelling Ekman layers to provide the majority of this would require that $\kappa_v' < 0.5$, which could be achieved by making $U > 0.05$ m s^{-1} and maintaining other parameters at the levels given in Table 1. As a second example, consider abyssal waters (4000–5000 m) where $\kappa_v' \approx 0.1$ (Table 1). For the conditions listed in Table 1, downwelling Ekman layers can easily account for this provided the typical contact time is less than, say, $10t_d$ (typically a few years in abyssal waters).

Even under more demanding conditions, such as $\kappa_v = 10^{-4}$ m^2 s^{-1} and $U = 0.05$ m s^{-1}, the required mixing can be achieved for contact times less than a couple of months. While there are clearly significant uncertainties in this type of analysis, the results demonstrate that downwelling Ekman layers are potentially an important mixing mechanism.

One advantage of the Ekman layer mixing equation (9) over the shear mixing equation (1) is that there is no need to assume a value for the mixing efficiency Γ. Furthermore, Γ can be explicitly calculated for downwelling Ekman layers as follows: The energy dissipated per unit area within the boundary layer after a boundary contact period t is

$$\int_0^t \rho C_D u^3 \, dt = \rho C_D U^3 t_d \left\{ \frac{1}{2}\left(\frac{h}{h_d}\right)^2 - \frac{1}{3}\left(\frac{h}{h_d}\right)^3 \right\}, \quad (12)$$

after substitution of (2) and (4). The corresponding increase in potential energy per unit area is given by (7), which when divided by (11) yields the average mixing efficiency up to time t:

$$\Gamma(t) = \frac{h}{3h_d - 2h}. \quad (13)$$

Figure 4 shows the growth in average efficiency with the time that water parcels are in contact with the boundary [Eq. (13)]. It is important to note that, while the average efficiency increases monotonically, there is a corresponding fall in the actual amount of mixing (Fig. 3). Most of the mixing occurs within the period $t < 3t_d$, by the end of which efficiencies have climbed to around $\Gamma = 0.4$. Any further mixing by this process is very slow and likely to be dominated by other processes so that efficiencies are not likely to approach unity. However, the theory does suggest that efficiencies are potentially much higher than values generally assumed for shear-driven boundary mixing ($\Gamma < 0.1$) and comparable to those found in the ocean interior ($\Gamma = 0.2$) by Osborn (1980) and Oakey (1982).

The arguments presented above indicate that boundary mixing associated with downwelling Ekman flows has the potential to contribute very significantly to deep ocean mixing. This is mainly due to the high efficiency of the mixing mechanism, particularly compared to tra-
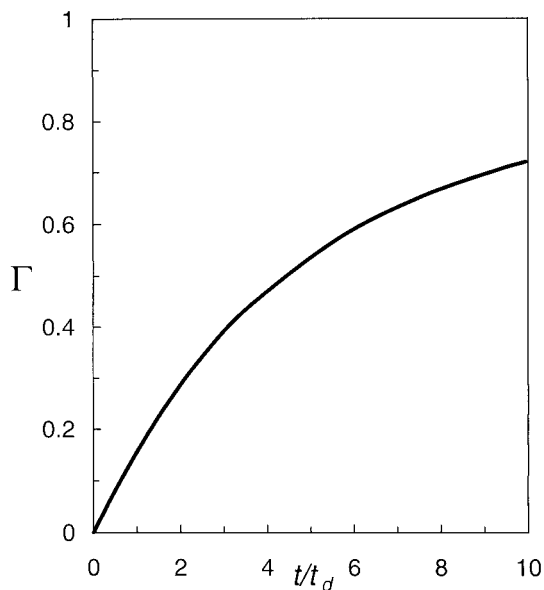
FIG. 4. Development of the theoretical mixing efficiency for downwelling favorable flows.

ditional shear-driven mixing. A question remains as to whether these theoretical efficiencies are realizable. While we cannot provide a definitive answer for the ocean at this time, it will be demonstrated below that results from a simple laboratory experiment tend to support the theoretical estimates.

4. Laboratory experiments

The theoretical growth rate of mixing efficiency is dependent on C_D (through t_d in Fig. 4), which is not easily scaled in the laboratory. However, the asymptotic efficiency associated with extended boundary contact (denoted here by Γ_∞) should be independent of C_D, as well as N, f, U, and θ [Eq. (13)]. It has already been noted that Γ_∞ is not expected to approach unity in a real flow and the laboratory results provide an independent

estimate, which may possibly be directly applicable to the ocean. They also allow direct comparison of mixing efficiencies for flows that are upwelling favorable (shear mixing only) and downwelling favorable (hydrostatic instability) within a single system.

The experiments were conducted on a rotating stratified flow over an axisymmetric sloping bottom. The general approach was similar to the stratified spinup experiments of MacCready and Rhines (1991). However, they focused on the Ekman layer shutdown and spinup timescales, whereas the emphasis here is on modification of the stratification by mixing during both spinup and spindown, and estimation of mixing efficiencies.

The experimental facility is shown schematically in Fig. 5. A conical shaped container with an inner slope of $\theta = 30°$ and outer slope of $\theta = 6°$ was mounted on a rotating table. For each run it was filled with salt stratified water to an approximate depth of either $H = 15$ cm (inner slope only) or $H = 24$ cm (inner and outer slope), while being spun up toward solid body rotation. The system was allowed to rotate for 10–15 hours before a density profile was recorded. The background rotation was then changed by an increment $\Delta\Omega$ to a final rate $\Omega = f/2$ within one inertial period. Density profiles were recorded during the spinup or spindown process until the system was again near solid body rotation. The elapsed time between the first and last profiles was always very much less than the timescale for molecular diffusion of salt.

Qualitative differences between upwelling and downwelling favorable flows can be seen in Fig. 6, which shows streaklines generated by potassium permanganate crystals within the boundary layer for both spinup and spindown events. During spinup, the boundary layer flow initially had an upslope component, which decayed to zero over a vertical distance of order h. Following this shutdown of the Ekman pumping, the flow was nearly azimuthal throughout the water column. The spindown process was vastly different from spinup, with downslope pumping resulting in static instability and overturning. Three-dimensional turbulent mixing of the
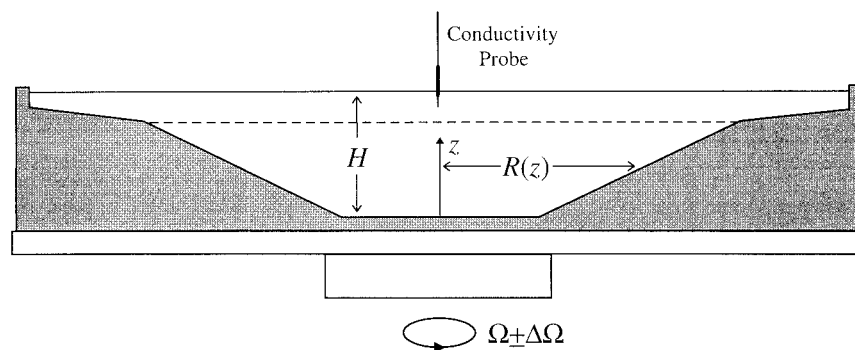

FIG. 5. Schematic side view of the rotating laboratory experiment. Experiments on a single slope were filled with salt stratified water to the level of the dashed line, while those on two slopes were filled to the solid line.
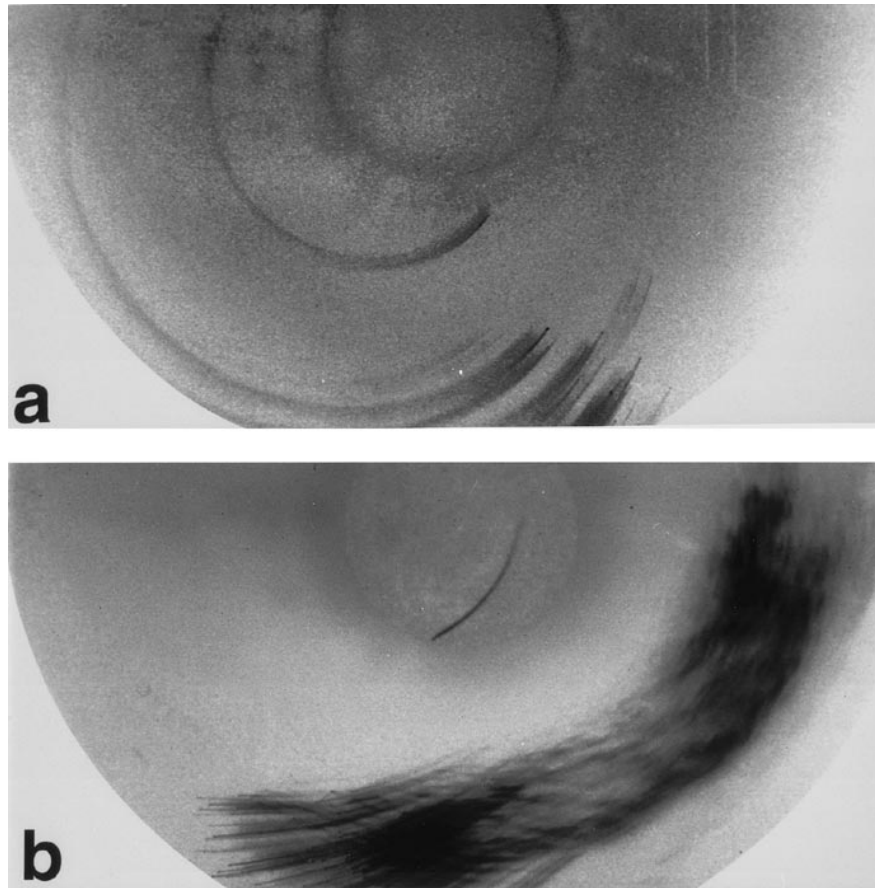
FIG. 6. Dye streaks produced by potassium permanganate crystals in the bottom boundary layer. The experiments corresponded to (a) spinup with $f = 3.0$ s^{-1} and $\Delta\Omega = 0.25$ s^{-1}, giving Ro = 0.083, and (b) spindown with $f = 2.5$ s^{-1} and $\Delta\Omega = 0.25$ s^{-1}, giving Ro = 0.10. In both cases $N = 1.7$ s^{-1} over most of the depth with weaker stratification near the surface. In (a) the dye streaks maintain their form while migrating up the slope, whereas in (b) they vigorously mix into a diffuse cloud after migrating a small distance down the slope.

permanganate tracer was very clear in video images and is also revealed in Fig. 6b by blurring of the streaks as dye is rapidly dispersed. The mixed fluid was advected by the alongslope flow while adjusting to the new geostrophic balance. It only collapsed toward the interior as the flow spun down through slow diffusion processes governed by molecular viscosity (MacCready and Rhines 1991).

While it was not feasible with this apparatus to make direct measurements resolving the boundary layer velocity structure, there is other substantial evidence that the Ekman layer shutdown process was occurring in the experiments. First, it has been previously shown in this type of experiment that the spinup and spindown of interior velocity fields are consistent with the shutdown process (MacCready and Rhines 1991). Second, the dye streak observations described above reveal exactly what would be qualitatively expected during the shutdown processes. The strong asymmetry between spinup and

spindown would be particularly difficult to explain through other known mechanisms.

Average mixing efficiencies have been calculated using density profiles recorded at the center of the tank. These calculations were only applied to profiles taken under conditions of solid body rotation before and after the change in background rotation, and therefore only provide the asymptotic mixing efficiency Γ_∞ $(t \gg t_d)$. There are three reasons why the temporal development of Γ was not calculated. First, it has already been noted that the laboratory timescales cannot easily be scaled to ocean flows. Second, it is only under solid body rotation that there are no horizontal density gradients, so the entire density field can be determined from a single vertical profile. Third, when moving between two states of solid body rotation the total dissipation is equivalent to the change in kinetic energy, which is easily determined.

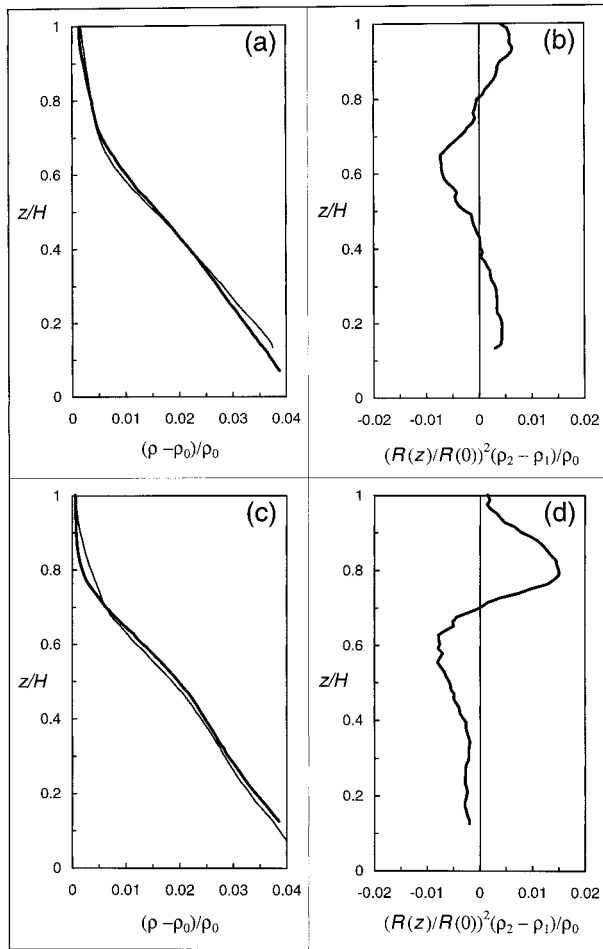Profiles taken before the change in backgound rota-

FIG. 7. Examples of density fields from the laboratory experiments with a single slope. (a) Density profiles before (thick line) and after (thin line) spinup (upwelling favorable). (b) The corresponding change in density profile during spinup weighted by the cross-sectional area of the container. (c) Density profiles before (thick line) and after (thin line) spindown (downwelling favorable). (d) The change in density profile during spindown weighted by the cross-sectional area of the container. Both experiments were characterized by $\theta = 30°$ and $N \approx 1.8$ s^{-1}. In (a) and (b) $f = 3.0$ s^{-1} and $\Delta\Omega = 0.5$ s^{-1}, while in (c) and (d) $f = 1.5$ s^{-1} and $\Delta\Omega = 0.25$ s^{-1}, giving a Rossby number of 0.17 in both cases.

tion, $\rho_t(z)$, and after adjustment to a new state of solid body rotation, $\rho_2(z)$, were used to calculate the asymptotic mixing efficiency from

$$\Gamma_\infty = \frac{\int_0^H \int_0^R \frac{1}{2} \frac{g(\rho_2 - \rho_1)^2}{(\partial\rho_1/\partial z)} r\, dr\, dz}{\int_0^H \int_0^R \frac{1}{2} \rho_1 (r\Delta\Omega)^2 r\, dr\, dz}, \qquad (14)$$

where r is the radial coordinate and $R(z)$ is the radius of the conical container. The potential energy term in the numerator is equivalent to the left-hand side of (7) taken from Gill (1979). The denominator is the initial kinetic energy, which in this case is equal to the change
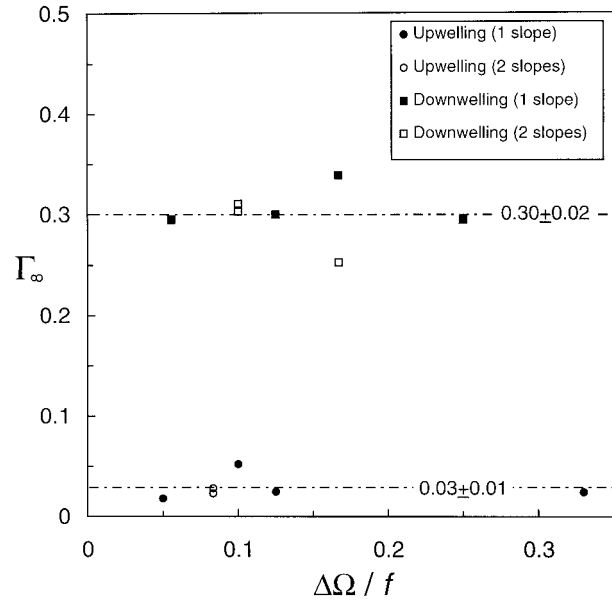

FIG. 8. Long term mixing efficiencies from all of the laboratory experiments. The upwelling favorable flows yielded efficiencies of around 3%, while the downwelling favorable flows yielded 30%.

in kinetic energy because the flow is returned to solid body rotation. When applying this formula to laboratory data, the vertical coordinate needed to be adjusted to take into account changes in elevation of the water column after a change in rotation rate due to centrifugal accelerations. A further check on this was provided by conservation of total salt between profiles.

Figure 7 shows typical examples of vertical density profiles before and after a spinup and similarly for spindown. As a measure of the vertical distribution of mixing, the change in density weighted by the horizontal area of the container at that height is also shown. In both cases the strongest mixing tends to occur toward the surface where alongslope velocities are greatest. However, there is more mixing at most depths in the downwelling favorable spindown experiments. This will now be quantified in terms of the mixing efficiency for the full range of experimental parameters.

A total of 13 experiments were conducted with depth-averaged N ranging from 0.8 to 1.9 s^{-1}, f from 1.5 to 4.8 s^{-1}, and $\Delta\Omega$ from 0.1 to 0.5 s^{-1} for both spinup and spindown runs. Mixing efficiencies calculated using (14) are plotted as a function of the Rossby number $\Delta\Omega/f$ in Fig. 8. In the spinup or upwelling favorable case, mixing efficiencies are very low with $\Gamma_\infty = 0.03 \pm 0.01$. This is not too surprising since the only mixing mechanisms available are shear instability and molecular diffusion. In contrast, mixing efficiencies were an order of magnitude larger for spindown or downwelling favorable flows with $\Gamma_\infty = 0.30 \pm 0.02$. There was also remarkably little variability and no detectable dependence on Rossby number or other parameters such as buoyancy frequency or bottom slope.

The finding that Γ_∞ is independent of laboratory flow conditions is consistent with the theoretical relation (13). It is also not too surprising that its magnitude of 0.3 is significantly less than the theoretical limit of 1. There are clearly other viscous processes capable of dissipating kinetic energy in the laboratory system, particularly over the longer timescales required to achieve very high efficiencies (Fig. 4). In any case, the experiments strongly support the premise that far more mixing occurs in downwelling favorable flows than upwelling favorable flows, as well as providing an independent estimate of long-term mixing efficiency.

5. Conclusions

Boundary mixing in downwelling favorable flows has been demonstrated to be far more effective than traditional shear instability mechanisms. Indeed, if the theoretical and/or laboratory results can be carried over directly to the real ocean, then it appears that this mechanism has the potential to explain a significant proportion of deep ocean mixing. This requires that mixed water be exchanged with the interior at the appropriate timescales. In particular, if water parcels tend to remain in contact with sloping boundaries for very long periods ($t \gg t_d$), there is a decline in both the average mixing within each parcel (Fig. 3) and the rate at which new parcels are brought into contact with the boundary. Details of the exchange mechanisms still require further investigation. However, since t_d is generally comparable to or larger than the relevant timescales of ocean variability, this factor is unlikely to limit mixing.

Figure 3 indicates that the most intense mixing occurs within the period $t < 3t_d$. For the case of the deep western boundary current in the North Atlantic, Garrett et al. (1993) note that t_d is typically around 100 days ($N = 1.2 \times 10^{-3}$ s^{-1}, $f = 7.3 \times 10^{-5}$ s^{-1}, $C_d = 2.5 \times 10^{-3}$ and $\sin\theta = 2 \times 10^{-2}$), so significant mixing might be expected over timescales up to a year. The current extends almost 4000 km along the lower continental slope with an average speed of around 0.2 m s^{-1}. This gives a boundary contact period of around 230 days, which is within the period of strong mixing. However, the tendency of the isopycnals to run parallel to the slope over much of its width may restrict the mixing to the upslope portion of the current where significant bottom density gradients exist (MacCready 1994).

Boundary mixing may also be significant in thermocline waters where t_d can range from a few days to a month or more (e.g., $N = 3 \times 10^{-3}$ s^{-1}, $f = 7.3 \times 10^{-5}$ s^{-1}, $C_d = 2.5 \times 10^{-3}$, and $\sin\theta = 2 \times 10^{-2}$ down to 1×10^{-2}). Flows such as the recirculating slope water north of Cape Hatteras (Hogg et al. 1986; Schmitz and McCartney 1993) provide a continuous supply of stratified water parcels, which are typically in contact with the slope for the order of a month. Other potentially significant mixing sites include straits, channels, and archipelagos, which are nearly always downwelling favorable along one side. An example with a particularly high throughput is the eastern side of the Straits of Florida, which has strong stratification, steep bathymetry, and a contact period of only a few days before being advected into open water by the Florida Current.

REFERENCES

Armi, L., 1978: Some evidence for boundary mixing in the deep ocean. *J. Geophys. Res.,* **83,** 1971–1979.
——, 1979: Effects of variations in eddy diffusivity on property distributions in the oceans. *J. Mar. Res.,* **37,** 515–530.
Garrett, C., 1979: Comments on ''Some evidence for boundary mixing in the deep ocean'' by Laurence Armi. *J. Geophys. Res.,* **84,** p. 5095.
——, 1990: The role of secondary circulation in boundary mixing. *J. Geophys. Res.,* **95,** 3181–3188.
——, and D. Gilbert, 1988: Estimates of vertical mixing by internal waves reflected off a sloping bottom. *Small-Scale Turbulence and Mixing in the Ocean: Proc. of the 19th Int. Liege Colloq. on Ocean Hydrodynamics,* J. C. J. Nihoul and B. M. Jamart, Eds., Elsevier, 405–424.
——, P. MacCready, and P. Rhines, 1993: Boundary mixing and arrested Ekman layers: Rotating stratified flow near a sloping boundary. *Annu. Rev. Fluid Mech.,* **25,** 291–323.
Gill, A. E., 1979: *Atmosphere–Ocean Dynamics.* Academic Press, 662 pp.
Gregg, M. C., 1987: Diapycnal mixing in the thermocline: A review. *J. Geophys. Res.,* **92,** 5249–5286.
——, 1989: Scaling turbulent dissipation in the thermocline. *J. Geophys. Res.,* **94,** 9686–9698.
Hogg, N. G., R. S. Pickart, R. M. Hendry, and W. J. Smethie Jr., 1986: The northern recirculation gyre of the Gulf Stream. *Deep-Sea Res.,* **33,** 1139–1165.
Ivey, G. N., 1987: The role of boundary mixing in the deep ocean. *J. Geophys. Res.,* **92,** 11 873–11 878.
Kato, H., and O. M. Phillips, 1969: On the penetration of a turbulent layer into stratified fluid. *J. Fluid Mech.,* **37,** 643–655.
Ledwell, J. R., A. J. Watson, and C. S. Law, 1993: Evidence for slow mixing across the pycnocline from an open-ocean tracer experiment. *Nature,* **364,** 701–703.
Lentz, S. J., and J. H. Trowbridge, 1991: The bottom boundary layer over the northern California shelf. *J. Phys. Oceanogr.,* **21,** 1186–1201.
MacCready, P., 1994: Frictional decay of abyssal boundary currents. *J. Mar. Res.,* **52,** 197–217.
——, and P. B. Rhines, 1991: Buoyant inhibition of Ekman transport on a slope and its effect on stratified spin-up. *J. Fluid Mech.,* **223,** 631–661.
——, and ——, 1993: Slippery bottom boundary layers on a slope. *J. Phys. Oceanogr.,* **23,** 5–22.
Matear, R. J., and C. S. Wong, 1997: Estimation of vertical mixing in the upper ocean at Station P from chlorofluorocarbons. *J. Mar. Res.,* **55,** 507–521.
Middleton, J. F., and D. Ramsden, 1996: Time-dependent boundary layers on the continental slope. *J. Geophys. Res.,* **101,** 18 061–18 077.
Munk, W. H., 1966: Abyssal recipes. *Deep-Sea Res.,* **13,** 207–230.
Oakey, N. S., 1982: Determination of the rate of dissipation of turbulent energy from simultaneous temperature and velocity shear microstructure measurements. *J. Phys. Oceanogr.,* **12,** 256–271.

Osborn, T. R., 1980: Estimates of the local rate of vertical diffusion from dissipation measurements. *J. Phys. Oceanogr.,* **10,** 83–89.

Phillips, O. M., J.-H. Shyu, and H. Salmun, 1986: An experiment on boundary mixing: mean circulation and transport rates. *J. Fluid Mech.,* **173,** 473–499.

Polzin, K. L., J. M. Toole, J. R. Ledwell, and R. W. Schmitt, 1997: Spatial variability of turbulent mixing in the abyssal ocean. *Science,* **276,** 93–96.

Ramsden, D., 1995: Response of an oceanic bottom boundary layer on a slope to interior flow. Part I: Time-independent interior flow. *J. Phys. Oceanogr.,* **25,** 1672–1687.

Schmitz, W. J., Jr., and M. S. McCartney, 1993: On the North Atlantic circulation. *Rev. Geophys.,* **31,** 29–49.

Thorpe, S. A., 1987: Current and temperature variability on the continental slope. *Philos. Trans. Roy. Soc. London,* **331A,** 183–194.

Trowbridge, J. H., and S. J. Lentz, 1991: Asymmetric behavior of an oceanic boundary layer above a sloping bottom. *J. Phys. Oceanogr.,* **21,** 1171–1185.